Altered Astrocyte Morphology and Vascular Development in Dystrophin-Dp71-Null Mice

Audrey Giocanti-Auregan,[1,2,3,4†] Ophélie Vacca,[2,3,4†] Romain Bénard,[2,3,4] Sijia Cao,[2,3,4] Lourdes Siqueiros,[2,3,4] Cecilia Montañez,[5] Michel Paques,[2,3,4,6] José-Alain Sahel,[2,3,4,6,7] Florian Sennlaub,[2,3,4] Xavier Guillonneau,[2,3,4] Alvaro Rendon,[2,3,4‡] and Ramin Tadayoni[2,3,4,8‡]

Understanding retinal vascular development is crucial because many retinal vascular diseases such as diabetic retinopathy (in adults) or retinopathy of prematurity (in children) are among the leading causes of blindness. Given the localization of the protein Dp71 around the retinal vessels in adult mice and its role in maintaining retinal homeostasis, the aim of this study was to determine if Dp71 was involved in astrocyte and vascular development regulation. An experimental study in mouse retinas was conducted. Using a dual immunolabeling with antibodies to Dp71 and anti-GFAP for astrocytes on retinal sections and isolated astrocytes, it was found that Dp71 was expressed in wild-type (WT) mouse astrocytes from early developmental stages to adult stage. In Dp71-null mice, a reduction in GFAP-immunopositive astrocytes was observed as early as postnatal day 6 (P6) compared with WT mice. Using real-time PCR, it was showed that Dp71 mRNA was stable between P1 and P6, in parallel with post-natal vascular development. Regarding morphology in Dp71-null and WT mice, a significant decrease in overall astrocyte process number in Dp71-null retinas at P6 to adult age was found. Using fluorescence-conjugated isolectin *Griffonia simplicifolia* on whole mount retinas, subsequent delay of developing vascular network at the same age in Dp71-null mice was found. An evidence that the Dystrophin Dp71, a membrane-associated cytoskeletal protein and one of the smaller *Duchenne muscular dystrophy* gene products, regulates astrocyte morphology and density and is associated with subsequent normal blood vessel development was provided.

GLIA 2015;00:000–000

Key words: dystrophin Dp71, astrocytes, retinal vascular development, angiogenesis

Introduction

Angiogenesis is a physiological process involving the growth of new blood vessels. In the retina, physiological angiogenesis during early development is essential for normal vision. Retinopathy of prematurity one of the leading cause of blindness in children involves abnormal retinal vessel

View this article online at wileyonlinelibrary.com. DOI: 10.1002/glia.22956

Published online Month 00, 2015 in Wiley Online Library (wileyonlinelibrary.com). Received June 23, 2015, Accepted for publication Dec 2, 2015.

Address correspondence to Dr Alvaro Rendon; Institut de la vision, 17 rue Moreau 75012 Paris, France. E-mail: alvaro.rendon@inserm.fr

From the [1]Ophthalmology Department, Avicenne Hospital, 125 Rue De Stalingrad, Bobigny, France; [2]Institut De La Vision, Sorbonne Universités, UPMC Univ Paris 06, UMR_S, 968, Paris, F-75012, France; [3]INSERM, U_968, Paris, F-75012, France; [4]CNRS, UMR_7210, Paris, F-75012, France; [5]Department of Genetics & Molecular Biology, Research Centre for Advanced Studies, IPN, Av. I.P.N. 2508, Mexico City, C.P., 07360, Mexico; [6]Centre Hospitalier National D'ophtalmologie Des Quinze-Vingts, DHU View Maintain, INSERM-DHOS CIC 1423, Paris, F-75012, France; [7]Fondation Ophtalmologique Rothschild, Paris, F-75019, France; [8]Ophthalmology Department, Hôpital Lariboisière, AP-HP, University Paris 7, Sorbonne Paris Cité, 2 Rue Ambroise Paré, Paris, 75010, France

[†]Audrey Giocanti-Auregan and Ophélie Vacca have contributed equally to this work.

[‡]Alvaro Rendon and Ramin Tadayoni have contributed equally to this work.

Conflict of Interest: AFM, CONACyT, ECOS Nord, Labex, AVOPH, ANR DysTher are public or non-commercial organizations. Allergan has offered an unrestricted grant to the laboratory used for this study.

Authors Also Disclose the following Conflict of Interests with Commercial Entities: Ramin Tadayoni is a board member of and consultant for Alcon, Switzerland; Novartis, Switzerland; Allergan, USA; Bausch and Lomb, USA; Alimera, USA; Bayer, Germany; FCI-Zeiss, France; Thrombogenics, Belgium; Roche, Switzerland; Genentech, USA; Zeiss, Germany. He has received lecture fees from Alcon, USA; Bausch and Lomb, USA; Novartis, Switzerland; Allergan, USA; Bayer, Germany; Alimera, USA, Zeiss, Germany, and meeting expenses from Novartis, Switzerland; Alcon, Switzerland; Allergan, USA; Bausch and Lomb, USA; Bayer, Germany; Alimera, USA. Audrey Giocanti-Auregan is consultant for Allergan, USA; Bayer, Germany, and Novartis, Switzerland. She has received lecture fees from Novartis, Switzerland; Allergan, USA; Bayer, Germany, and meeting expenses from Novartis, Switzerland; Alcon, Switzerland; Allergan, USA; Bayer, Germany, and Alimera, USA.

Additional Supporting Information may be found in the online version of this article.

development. Astrocytes are intimately involved in the formation, development, and function of central nervous system vessels (Ma et al., 2012). In the retina, astrocytes are believed to play an important role in the development of the mammalian retinal vasculature (Chan-Ling and Stone, 1991; Fruttiger et al., 1996; Hirota et al., 2011; Kubota and Suda, 2009; Ling and Stone, 1988; Ling et al., 1989; Scott et al., 2010; Stenzel et al., 2011). Shortly after birth, blood vessels are known to emerge at the optic disc and sprout radially just underneath the vitreal surface of the retina until they reach the peripheral margin (Fruttiger, 2007). The growing vessels are guided by an astrocyte network producing vascular endothelial growth factor (VEGF) (Fruttiger, 2007; Stone et al., 1995; West et al., 2005). In a second phase starting around postnatal day 6 (P6), the vascular branches also sprout downward into the retina to form additional plexus. In rodents, vascular sprouts grow down along Müller cell processes into the retina and turn sideways when they reach the inner and outer boundaries of the inner nuclear layer to establish two additional networks parallel to the primary plexus (Fruttiger, 2007). Retinal astroglial cells are only found in species with a vascularized retina, and are restricted to vascularized areas (Fruttiger, 2007; Fruttiger et al., 1996; Provis et al., 2000; Schnitzer, 1988). The formation of the primary vascular layer in the retina is closely associated with the underlying astrocytes that are present at birth on the retina surface from the optic nerve to the peripheral retina. Primary layer vessels are known to migrate on this pre-established network. Adhesion proteins produced by astrocytes such as R-cadherin, an adhesion molecule involved in neuronal cell guidance have been shown to be involved in the formation of the primary vascular layer in the retina. When R-cadherin expression is inhibited during retinal vascular development, vessel migration on the retina is compromised (Dorrell et al., 2002). Laminins, some extracellular matrix components of the internal limiting membrane (ILM), also appear to regulate retinal blood vessel growth and maintain vascular integrity.

Dystrophin 71 (Dp71), a membrane-associated cytoskeletal protein and one of the smaller *Duchenne muscular dystrophy* (*DMD*) gene products that is the core of the Dystrophin-Associated Protein (DAP) complex, links the intracellular actin cytoskeleton to the extracellular matrix. Studies on nervous tissue support the potential involvement of Dp71 in neuronal and glial cell functions (Aleman et al., 2001; Claudepierre et al., 2000; Dalloz et al., 2003; Daoud et al., 2009; Fort et al., 2008). Dp71 mRNA and protein have been shown to be expressed in different brain structures and cell types, including perivascular astrocytes, neurons in the hippocampus and olfactory bulb, cultured hippocampal neurons and forebrain astrocytes, and postsynaptic densities *in vivo*. It has been suggested that in the brain, the Dp71 protein located in the astrocyte perivascular end foot membrane, participates in water and K+ homeostasis and blood–brain barrier stabilization (Benabdesselam et al., 2010; Nico et al., 2003; Nicchia et al., 2004). In the retina, we have shown that the inwardly rectifying potassium channel Kir4.1 and the aquaporin 4 water channel (AQP4) associate with the Dp71-DAP dependent subcomplex at Müller cell endfeet (Fort et al., 2008) and that this complex subsequently associates with laminin through β-dystroglycan (Hirrlinger et al., 2011). Genetic inactivation of Dp71 (in Dp71-null mice) alters Kir4.1 and AQP4 distribution in Müller cells and this mislocation is associated with impaired retinal water regulation and retinal nerve cell vulnerability to transient ischemia. Moreover, the absence of Dp71 in mouse retina causes a breakdown of the blood–retinal barrier (BRB) (Sene et al., 2009) that is associated with retinal vascular inflammation, vascular lesions with increased leukocyte adhesion, and capillary degeneration (El Mathari et al., 2015). Given the localization of Dp71 around the vessels in adult mouse retina and its role in maintaining retinal homeostasis, we hypothesized that Dp71 could play a role in astrocyte and vascular development regulation.

Based on similarities between the brain and the retina, and the expression of Dp71 reported in brain astrocytes (Szabó et al., 2004), we first investigated using a dual immunolabeling whether or not Dp71 was expressed in retinal astrocytes. We found that Dp71 was expressed in wild-type (WT) mice from early developmental stages to adult stage. We then investigated astrocyte biological factors, which could underlie the role of Dp71. To this end, cytotopographical studies were performed in Dp71-null mice, including analysis of astrocyte density and morphology. We found that the absence of Dp71 resulted in a dramatic reduction in astrocyte density as early as at P6 compared with WT mice. Compared with WT mice, we found a significantly decreased overall process number in Dp71-null mouse retinas. We then hypothesized that the altered astrocyte phenotypes induced by the absence of Dp71 could impair the subsequent vascular development. We found that the vascular growth in Dp71-null mice was significantly reduced with a significant decrease in vessel density, number of their branches, and branching points. Taken together, these data support the assumption that Dp71 plays a crucial role in retinal vascular functions.

Materials and Methods

Animals

All experiments were done in compliance with the European Communities Council Directives (86/609/EEC) for animal care and experimentation (HMG). Mice were handled in accordance with the Association for Research in Vision and Ophthalmology (ARVO) statement for the use of animals in ophthalmic and vision research.

Dp71-null mice were obtained as described previously (Sarig et al., 1999) by replacing, via homologous recombination, most of the first and unique exon of Dp71 and a small part of Dp71 first intron by a sequence coding a β-galactosidase (β-gal)-neomycin-resistance chimeric protein (β-geo). Dp71 expression was abolished without interfering with the expression of other *DMD* gene products. Moreover, the expression of the inserted promotorless *β-geo* gene was under the control of the *Dp71* promoter. Dp71-null mice and their WT littermates (C57BL6J) were bred in our laboratory.

Retinal Flat-Mount Preparations

The exact birth time of mice was monitored by checking twice a day the cages for birth. Mice were sacrificed at specific terms (P0, P3, P6, P9, P12, or Adult stage, i.e., 8-week-old mice) and they were enucleated. Eyes were then fixed in 4% paraformaldehyde (PFA) for 1 hour. Retinas were dissected free from surrounding tissues, incubated in methanol (−20°C) for 10 minutes, blocked with 3% normal goat serum (NGS)—0.1% Triton—1× Phosphate Buffered Saline (PBS) for 1 hour, and incubated overnight at +4°C in 0.1% Triton X-100—1× PBS with different primary antibodies or markers. After three washes (1× PBS for 5 minutes), retinas were incubated with the appropriate fluorescence-conjugated secondary antibody (1:500; in saturation buffer, Life Technologies) for 1 hour at room temperature then washed three times and mounted on slides with aqueous mounting medium (Thermo Scientific). Antibodies and molecular markers included fluorescence-conjugated lectin *Griffonia simplicifolia* (1:100; Sigma-Aldrich) and rabbit anti-glial fibrillary acidic protein (GFAP, 1:1,000; Dako). In each case, secondary control incubations were performed to determine labeling specificity.

Retinal Cryosections

Mice were sacrificed at different time points. Enucleated eyes were fixed in 4% PFA, transferred into 30% sucrose—1× PBS overnight at +4°C, and embedded in optimal cutting temperature compound (OCT cryomatrix, Thermo Scientific). Ten-micrometer frozen sections were washed with PBS, and blocked for 1 hour with 0.1% Triton X100—1% BSA—1× PBS before overnight incubation at +4°C with a homemade (D. Mornet, France) rabbit anti-dystrophin H4 (1:2,000) no commercially available (Fabbrizio et al., 1994), mouse monoclonal anti-GFAP (1:500; Sigma-Aldrich), fluorescence-conjugated lectin *Griffonia simplicifolia* (1:100; Sigma-Aldrich) antibodies. Sections were then incubated with a goat anti-rabbit and a goat anti-mouse secondary antibody (1:500; Life Technologies) for 1 hour at room temperature. Cell nuclei were stained with 4′,6-Diamidino-2-phenylindole dihydrochloride (DAPI, 300 nM; Life Technologies). In each case, secondary control incubations were performed to determine labeling specificity.

Astrocyte Isolation

Eyes were enucleated before being dissected in PBS. Both retinas were then removed and incubated in PBS containing 3% Papain for 30 minutes at +37°C. Retinas were washed three times with PBS then fixed with 4% PFA for 10 minutes at room temperature. Once the PFA removed, the retinas were again washed two times with 1× PBS. Cells were then mechanically dissociated by trituration with a pipette tip. Cell suspensions from WT and Dp71-null mice were diluted to the same concentrations after counting using a hemocytometer.

For immunolabeling, cells were freshly separated and deposited on a slide placed on a warm plate at +37°C for adherence. They were then rehydrated with 1× PBS and incubated with 1× PBS—0.1% Triton X-100 for 5 minutes. After saturation for 1 hour in a 1× PBS solution containing 0.1% Tween 20—3% NGS (Normal Goat Serum)—1% BSA (Bovine Serum Albumin), cells were incubated with primary antibodies for 2 hours at room temperature or overnight at +4°C. Cells were then washed three times with a 1× PBS solution containing 0.1% Tween 20 and incubated for 1 hour with the secondary antibody (Alexa coupled). This incubation was followed by two washes with 1X PBS solution containing 0.1% Tween 20 and one wash with distilled water. Cells were subsequently mounted between slides and coverslip with fluorsave (Thermo Scientific).

Counting of Retinal Astrocytes

Dissociated cells were labeled with a polyclonal anti-GFAP antibody (Glial fibrillary acidic protein, 1:1,000, Dako), a monoclonal anti-GS antibody (Glutamine Synthetase, 1:2,000, Millipore), and DAPI (1:1000, Life Technologies). After mounting, nine fields on each slide were captured under 10× objective with a fluorescence microscope. DAPI-stained nuclei in each field were counted using Fiji software and the GFAP positive and GS negative stellar-like astrocytes were counted manually. Results from all nine fields on each slide were summed to calculate the astrocyte density.

RNA Isolation and Real-Time Quantitative Polymerase Chain Reaction (RT-PCR)

Messenger ribonucleic acid (mRNA) level of several proteins was measured by real-time qRT-PCR at two or three development time points (P1, P3, and P6). For each time point, retinas were dissected in RNase-free medium and frozen at −80°C. Subsequently, retinas were pooled and total RNA was extracted with Trizol reagent (Invitrogen) according to the manufacturer's instructions. RNA integrity was verified before reverse transcription through visualization of the 28s and 18s ribosomal RNA bands.

Total RNA was reverse transcribed using Superscript First-Strand Synthesis System for RT-PCR (Invitrogen) with random hexamers (Invitrogen) according to the manufacturer's instructions. Briefly, 1 μL of random hexamers and 1 µL of dNTP mix were added to 9 μL of extracted RNA and incubated at +65°C for 5 minutes. After adding 2 μL of 10× RT buffer, 4 µL of 25 mM $MgCl_2$, 1 μL of RNaseOUT, 2 μL of 0.1 M DTT, and 1 μL Superscript III RT (50 U/µL), a thermocycler (Applied Bio systems) was used to incubate the samples at room temperature for 10 minutes, at +42°C for 50 minutes and at +70°C for 15 minutes.

Subsequently, 10 ng of the resulting cDNA were added to Fast Start universal SYBR Green Master Mix (Rox) (Roche) and placed into the StepOnePlus Real-Time PCR System (Applied Bio systems) for 40 cycles. Forward and reverse primers were designed using Primer 3 software (Table 1).

PCR amplification consisted of an initial denaturation step at +95°C for 10 minutes, followed by 40 cycles of denaturation at

TABLE 1: Forward and Reverse Primer Sequences

Gene	Forward primer	Reverse primer
Dp71	ATGAGGGAACACCTCAAAGGCCACG	TCTGGAGCCTTCTGAGCTTC
R-Cadherin	GACGTGAGGGACAACATCCT	CTGTTGCAGCTGGCTGAG
VEGF-A	ATCTTCAAGCCGTCCTGTGT	GCATTCACATCTGCTGTGCT
β-Actin	GCTCTTTTCCAGCCTTCCTT	CTTCTGCATCCTGTCAGCAA
RPS26	AAGTTTGTCATTCGGAACATT	AGCTCTGAATCGTGGTG

+95°C for 15 seconds and annealing and extension at +60°C for 1 minute. Melting curve analysis (+60°C to +95°C increment at +0.3°C) was used to determine the melting temperature of specific amplification products and the possible formation of primer dimers. These experiments were independently repeated at least three times. Real-time quantitative RT-PCR was performed to quantitatively assess the mRNA level of Dp71, and VEGF-A. β-Actin was used as an internal control for normalization purposes. Following the generation of the standard curve, the PCR efficiency was determined for each gene. The $2^{-\Delta Ct}$ method was used for normalization.

Image Analysis

Images of astrocytes and vessels were captured using a fluorescence microscope (Leica Z6 APO Microsystem Inc., Deerfield, IL) and a confocal microscope (TCS SP2, Leica) for captured localization of Dp71 in the retina. For vascularization development, the retina surface covered by vessels was measured and expressed as a percentage of the entire retina surface to obtain the vascularized area. Measurements were made using Photoshop 7.0 software.

To quantify astrocyte and vessel morphology, flat-mounted retinas from P6 and adult mice were analyzed using Fiji algorithms on two-dimensional (2D) images. Analyze Skeleton plugin (Arganda-Carreras et al., 2010) tags all pixels in a skeleton image then counts all its junctions, branches, and measures their mean length. Eight-bit gray-scale images were open with Fiji software. Image noise was removed by processing a smooth filter (Plugins > Process > Smooth (3D) > Gaussian Method—1 sigma). Then, images were binarized (Image > Adjust > Threshold > Apply) and the skeleton was extracted from binary images using Skeletonize (2D/3D) (Fig. S1, Supp. Info.). Figure S1 in Supporting Information shows the protocol used for astrocyte vessel morphology analysis. Finally, the resulting skeletons were analyzed on the 2D images using Analyze Skeleton (2D/3D). For each skeleton, the number of branches (astrocyte processes or number of branches), number of actual junctions (astrocyte intersections or branching points), and mean branch length (process or vessel length) were investigated. Results are expressed as a number per mm^2 or length (μm) per mm^2.

To quantify vessel density, four epifluorescence images were taken per retina, using the same settings, with a DM5500 Leica microscope. Then, three fields per image were taken near the migration front. Thus, 12 fields per retina were analyzed and fluorescence areas were quantified using Fiji software.

Statistical Analyzes

All data were analyzed using the non-parametric Mann–Whitney test ± SEM except for astrocyte morphology quantification where an unpaired t test ± Standard Deviation (SD) was used. Graph pad prism 6 software was used for all analyzes and statistical significance was set at $P < 0.05$.

Results

Dp71 Localization in Astrocytes

The expression of Dp71 in retinal astrocytes was investigated. Retinal sections from WT mice were double immunolabeled with antibodies to Dystrophin (H4) and GFAP. The anti-Dystrophin antibody H4 revealed a signal around blood vessels and at the ILM that colocalized with GFAP signal in astrocytes from P6 and 2-month (2M) old mice (Fig. 1A, B). To confirm this observation, retinal cells from adult WT and Dp71-null mice were dissociated and double immunolabeled with the same antibodies. Dystrophins and GFAP colocalized in dissociated astrocytes from WT retinas. In astrocytes from Dp71-null retinas, only the GFAP signal was obvious (Fig. 1C). These observations confirm that Dp71 is expressed in retinal astrocytes.

Dp71 Deletion Affects Astrocyte Morphology and Density

The morphology of GFAP+ retinal astrocytes was investigated in Dp71-null mouse retinas. Figure 2A–C show clearly a conspicuous morphological dissimilarity in the density of astrocytes present around the vessels as well as an apparent decrease in the number of astrocyte processes in P6 and 2M old Dp71-null mice compared with WT mice. At higher magnification, an obvious morphological difference in shape was observed between WT and Dp71-null astrocytes (Fig. 2C). In Dp71-null mice, a narrow contact was observed between astrocyte end feet and endothelial cells while the contact was wider in WT mice.

The number of processes and ramification size in WT and Dp71-null retinas were quantified in a rectangular area at

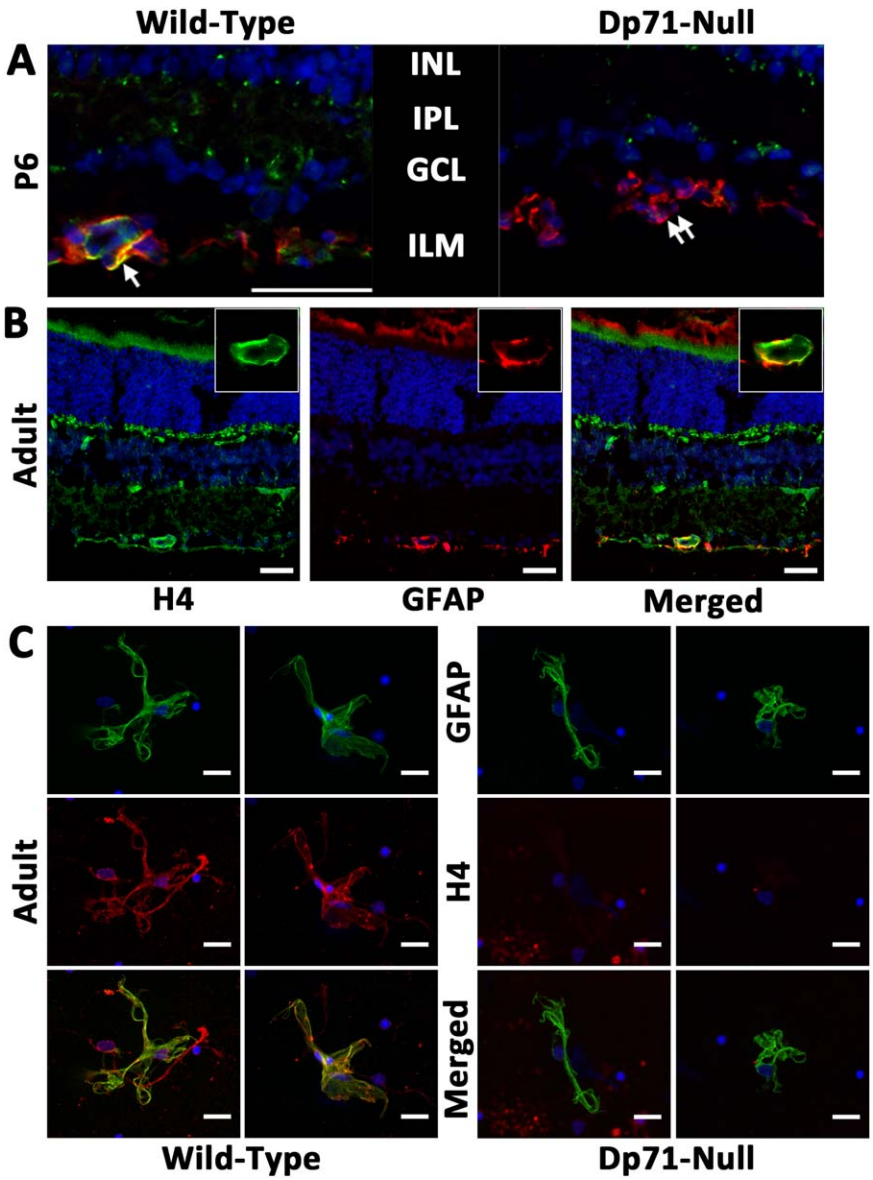

FIGURE 1: Localization of Dystrophin-Dp71 in Astrocytes. (A) At P6, Dp71-null mice retina cryosection presents no significant H4 staining (*green*) below the limit of ganglion cells layer (*double arrow*). However, WT mice retina displays a clear H4 staining at the inner part of the retina (*single arrow*) co-localizing with GFAP staining (*red*) at this stage of retinal development (scale bar = 50 μm). (B) In adult WT retinal cryosection, H4 staining (*green*) also co-localizes with GFAP staining (*red*) (scale bar = 50 μm). At high magnification (*white rectangle*), H4 staining co-localizes with astrocytes processes surrounding vessels. (C) In isolated astrocytes, H4 staining (*red*) co-localizes with GFAP staining (*green*) in WT adult mice whereas in Dp71-null mice, H4 staining is absent (scale bar = 5 μm).

P6 and 2M (Fig. 2D,E). The number of processes was significantly reduced in Dp71-null astrocytes compared with WT astrocytes in neonate and adult retinas. In WT astrocytes, the number of processes increased over time. Conversely, the number of processes was stable in Dp71-null astrocytes in neonate and adult retina. However in WT and Dp71-null mice, no significant difference in process length was observed between two bifurcations at P6 or 2M. To further examine the morphological changes in Dp71-null astrocytes, the number of times a process segment crossed over another one was measured. A significant decrease in the number of intersections was observed in adult Dp71-null mice compared with WT mice, meaning that the mature astrocyte network was less complex and less developed when Dp71 was not expressed.

The potential impact of the absence of Dp71 was also assessed on the retinal density of astrocytes by counting manually the GFAP positive astrocytes per unit area of Dp71-null versus WT retinas at different ages, from P6 to adult stage. The number of retinal astrocytes decreased with age in

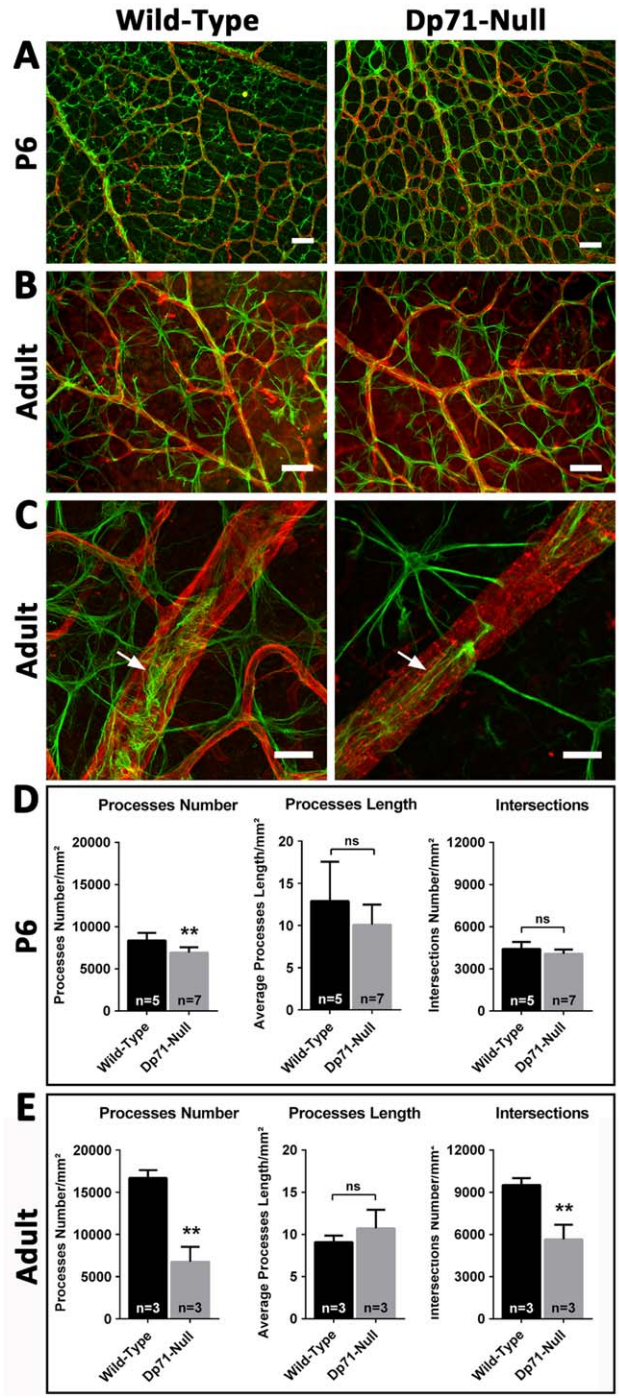

FIGURE 2: Astrocytes morphology of WT and Dp71-null mice retina. (A,B) Visualization of the astrocyte network labeled with anti-GFAP antibody (*green*) and of the vascular network labeled with lectin GS (*red*) at post-natal day 6 (A) and at the adult age (B) (scale bars = 25 μm). (C) Higher magnification of astrocyte network around major vessels in adult WT and Dp71-null mouse retinas. Flat-mount retinas labeled with lectin GS (*red*) and anti-GFAP antibody (*green*). Note the changes in morphology of retinal astrocytes in A and B in Dp71-null mice compared with control. In C, the white arrows are pointing out the different morphology of the astrocyte endfeet. (D, E) Quantification of the astrocytes processes number, of their length and of their intersection number on images such as A for P6 ($n = 5$–7) and B for adults ($n = 3$), using Analyze Skeleton plugin of Fiji software (Unpaired *t* test ± SD; $^{**}P < 0.01$) (see Fig. S1, Supp. Info.).

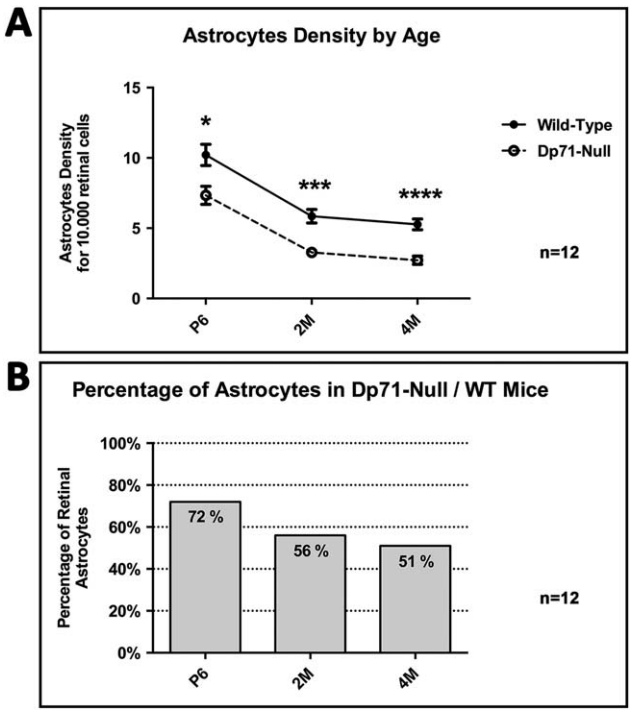

FIGURE 3: Astrocytes density of WT and Dp71-null mouse retinas at different ages. (A) Astrocytes density at P6, 2M and 4M after birth, expressed as the astrocyte number per 10000 retinal cells. The number of retinal astrocytes decreases with age in WT and Dp71-null mice. Number of GFAP+ retinal astrocytes decreases significantly in Dp71-null mice compared with age-matched WT mice at all timepoints. (B) Percentage of GFAP+ retinal astrocytes in Dp71-null mice compared with age-matched WT mice. The astrocyte number decreases with age in Dp71-null mice. Detailed information is provided in Table 2. (Mann–Whitney test ± SEM; $^{*}P < 0.05$, $^{***}P < 0.001$, $^{****}P < 0.0001$; $n = 12$).

Dp71-null and WT mice (Fig. 3A). Moreover, as shown in Fig. 3B, the deletion of Dp71 aggravated the age-dependent astrocyte loss: at P6, the retinal astrocyte density was 28% less in Dp71-null retinas and at 2M and 4M the astrocyte density was reduced by 44% and 49%, respectively. Statistical differences are detailed in Table 2.

Delayed Angiogenesis in Dp71-Null Retina and Dp71 Development

Based on our first findings, Dp71 could play a role in the regulation of astrocyte density and morphology. The postnatal retinal vessel development was thus compared between WT and Dp71-null mice. In WT mice, the development of the inner vasculature was labeled with lectin *Griffonia simplicifolia* (GS) and results showed that at P0, 3% of the total retinal surface was covered by vessels, with progressive growth of the first vessel layer covering 23% at P3 and 65% at P6 (Fig. 4A,B). In Dp71-null mice, the vasculature was comparable to that in WT mice at P0 (2%); however quantification in 29 separate litters at P3 revealed that 16% of the retinal surface

TABLE 2: Retinal Astrocyte Density

	P6		2M		4M	
	WT	**Dp71-null**	**WT**	**Dp71-null**	**WT**	**Dp71-null**
Mean	10.21	7.345	5.847	3.274	5.270	2.723
SD	2.625	2.039	1.684	0.7276	1.328	1.047
SEM	0.7578	0.6448	0.4862	0.21	0.3834	0.3021
N	12	10	12	12	12	12
P value	P = 0.0205*		P = 0.0001***		P < 0.0001****	

SD, standard deviation; SEM, standard error of mean; *N*, number of trials. Mann–Whitney test was used. All values are expressed as the density of astrocytes for 10.000 retinal cells.

was covered, a value significantly less than that found in WT mice. This corresponded to a subtle, but significant, delay in angiogenesis. Moreover, at P6 this difference increased, showing a dramatic reduction in vascular network spreading by 37% in Dp71-null mice and 65% in WT mice (Fig. 4A,B). The deep plexus developed later with a highly significant difference at P12. However, despite the difference in vasculature development, the retinal surface appeared totally covered by vessels in adult Dp71-null mice (Fig. S2, Supp. Info.).

A Dp71 development analysis of Dp71 mRNA level was performed in the retina of WT mice using real-time qPCR. Figure 4C shows that Dp71 mRNA was expressed at P1 and its expression level did not change until P6.

Impacts of Dp71 Deletion on Astrocyte Migration and Retinal Angiogenesis and Vascular Plexus Guidance

To improve our understanding of the relationship between astrocytes and the development of the mouse retinal vasculature, the retina of Dp71-null mice was examined at various development stages. Using a GFAP polyclonal antibody, a nearly complete astrocyte network covering the entire retina was observed at birth. At P3, fluorescent cells were visible in the vicinity of the retinal periphery edges in both WT and Dp71-null mice (Fig. 5A), suggesting that the absence of Dp71 did not interfere with the postnatal astrocyte migration during retinal development.

The double immunostaining of GFAP and lectin GS allowed visualizing the pattern of retinal vessels and retinal astrocytes. As shown at P6 (Fig. 2), a conspicuous dissimilarity in astrocyte density and morphology was observed at P3 between WT and Dp71-null mouse retinas (Fig. 5B—GFAP). The close examination of the superficial vascular plexus (Fig. 5B—Lectin) showed that the absence of Dp71 also induced vasculature dissimilarity in terms of vessel morphology and density compared with WT mouse retinas. Merging lectin GS and GFAP images (Fig. 5C—merge) showed that endothelial cells were always associated with the underlying astrocytes in WT and Dp71-null mice despite astrocyte and vasculature malformation. This observation suggest that the initial mechanism involved in endothelial cell guidance signals during their migration through the underlying astrocyte template during development, was not impaired in the absence of Dp71.

The possible impairment in the vasculature plexus was also studied in the absence of Dp71. Flat-mount retinas were analyzed at P6, that is, when most of the primary network is usually formed in WT mice. As described for astrocytes, the vascularization area, number of branches, branching points, and vessel length were measured in a rectangular area (Fig. 6A, B). A significant decrease in vasculature density, number of branches as well as branching points was found in Dp71-null mice compared with WT mice (Fig. 6C–E). However, due to the decrease in branching points, the vessel length was dramatically increased (Fig. 6F). Using qRT-PCR, the mRNA level of R-Cadherin, which is required for retinal endothelial cell guidance, was quantified 3 days after birth. R-cadherin mRNA level was lower at P3 in Dp71-null mice (Fig. 7A), probably due to a lower retinal astrocyte density. These data indicate that the impaired vasculature and delayed retinal vascular plexus maturation in Dp71-null mice could be due to a disruption of the astrocyte template.

Impaired VEGF Expression in Dp71-Null Mice

In order to assess the impact of Dp71 deletion on astrocyte morphology and density, we measured VEGF-A, mRNA level by qRT-PCR at P3 in WT and Dp71-null mice, a mediator of astrocyte-vessel interaction during retinal vasculature development. Dp71 deletion was associated with a significant increase in VEGF-A mRNA level at P3 in Dp71-null mouse retinas compared with WT mice (Fig. 7B), indicating that VEGF produced by astrocytes was not directly involved in the angiogenesis delay observed in Dp71-null mice.

Discussion

Understanding the retinal vascular development is crucial because many retinal vascular diseases such as diabetic retinopathy or retinopathy of prematurity are among the leading causes of blindness. To date, an increasing number of molecules are known to contribute to the formation of the primitive vascular plexus, leading to an organized architecture (Gariano and Gardner, 2005). Among the Dystrophin superfamily members, the Dystrophin Dp71 has been found in the ILM and around blood vessels in adult mouse retinas (Howard et al., 1998). Dp71 is mainly and strongly expressed in Müller glial cells and is critical for the clustered localization of Kir4.1 and AQP4 (Pannicke et al., 2002). The role of Dp71 in maintaining retinal homeostasis led us to assume that Dp71 could play a role in astrocyte and vascular development regulation. In the mouse retina, it is well established that astrocytes act as the primary proangiogenic cell type required for the development of the retinal vascular system. Here we showed that Dp71 was expressed in retinal astrocytes suggesting that Dp71 could be necessary to sustain the role of astrocytes in the formation of the retinal vascular plexus. We found that the vascular growth in Dp71-null mice was significantly reduced with a significant decrease in vessel density, number of their branches and branching points. A possible explanation of a lower vessel density in Dp71-null mice could have been a lower density of retinal neurons, leading to a decrease of metabolic needs and thus impacting the vessel density. However, the reduction of vessel density, number of branches, and branching points does not seem to be related to the altered metabolic needs of retinal neurons for the following observations: (i) Dp71 is not expressed in retinal neurons (Wersinger et al., 2011), (ii) in absence of Dp71 there is no reactional gliosis (Sene et al. 2009) suggesting that there is no neuronal damage, (iii) there is no significant difference of the number of ganglion cell between WT and Dp71-null retinas (Dalloz et al. 2003), (iv) moreover, as shown in Fig. S3, Supporting Information, the quantification of the bipolar cells on retinal sections between Dp71-null and control mice is not significantly different.

In the central nervous system, it has been demonstrated that an astrocyte-derived template is crucial for the development of angiogenesis. In the brain, the inhibition of astrogliogenesis results in a reduced astrocytic coverage, and subsequently in a reduced vessel growth and branching during the postnatal

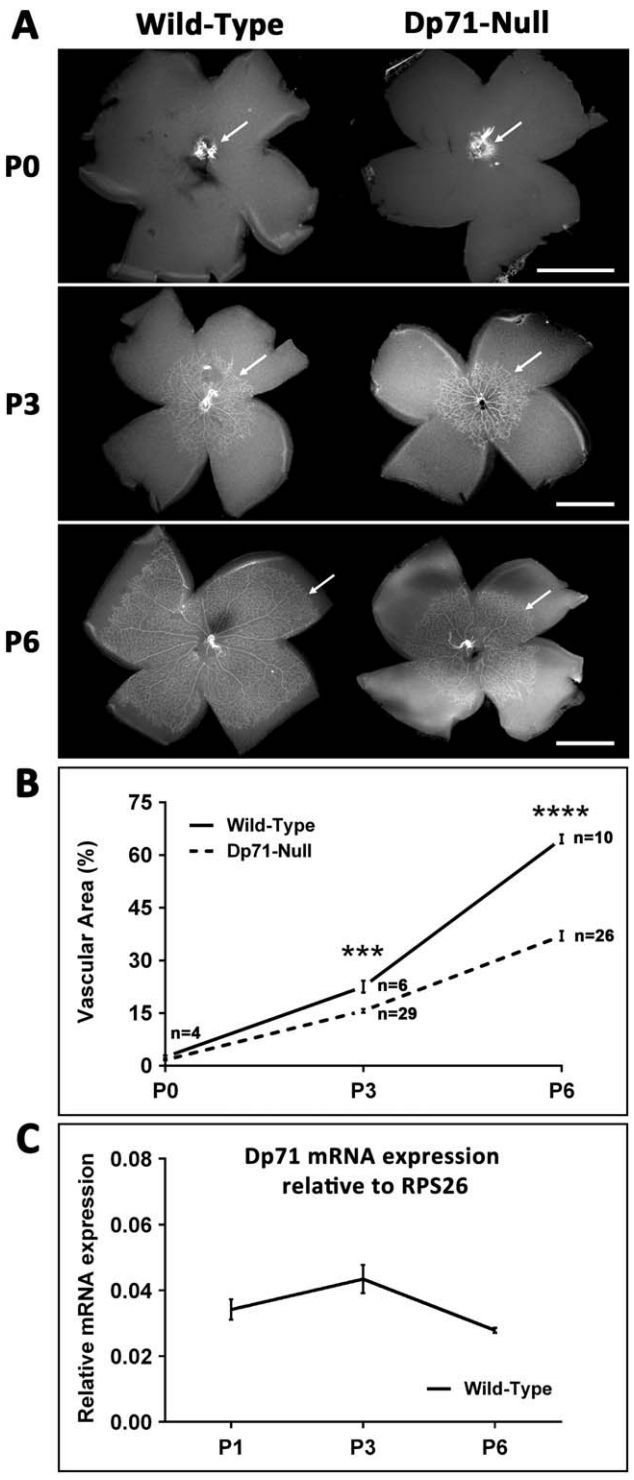

FIGURE 4: Formation of the superficial vascular plexus in WT and Dp71-null mice retinas. (A) Visualization of the retinal vasculature in WT and Dp71-null mouse retinas using lectin GS staining. At birth (P0), mouse retinal vasculature is absent. Then, vessels grow from the optic nerve to the retinal periphery. At P3 and remarkably at P6, vascular area of Dp71-null mouse retina is smaller compare to WT mice (*arrows*) (scale bars = 100 μm). (B) Representation of the superficial vascular development delay. Data show significantly smaller vascular areas at P3 and P6 in Dp71-null mice (Mann–Whitney test ± SEM; ***$P < 0.001$, ****$P < 0.0001$; n = on the graph). (C) Dp71 mRNA expression level relative to the ribosomal protein S26 (RPS26) at P1, P3, and P6 in the WT retina (Mann–Whitney test ± SEM; $n = 4$). Between P1, P3, and P6, there was no significant difference. In the Dp71-null mice retina, there was no Dp71 mRNA expression.

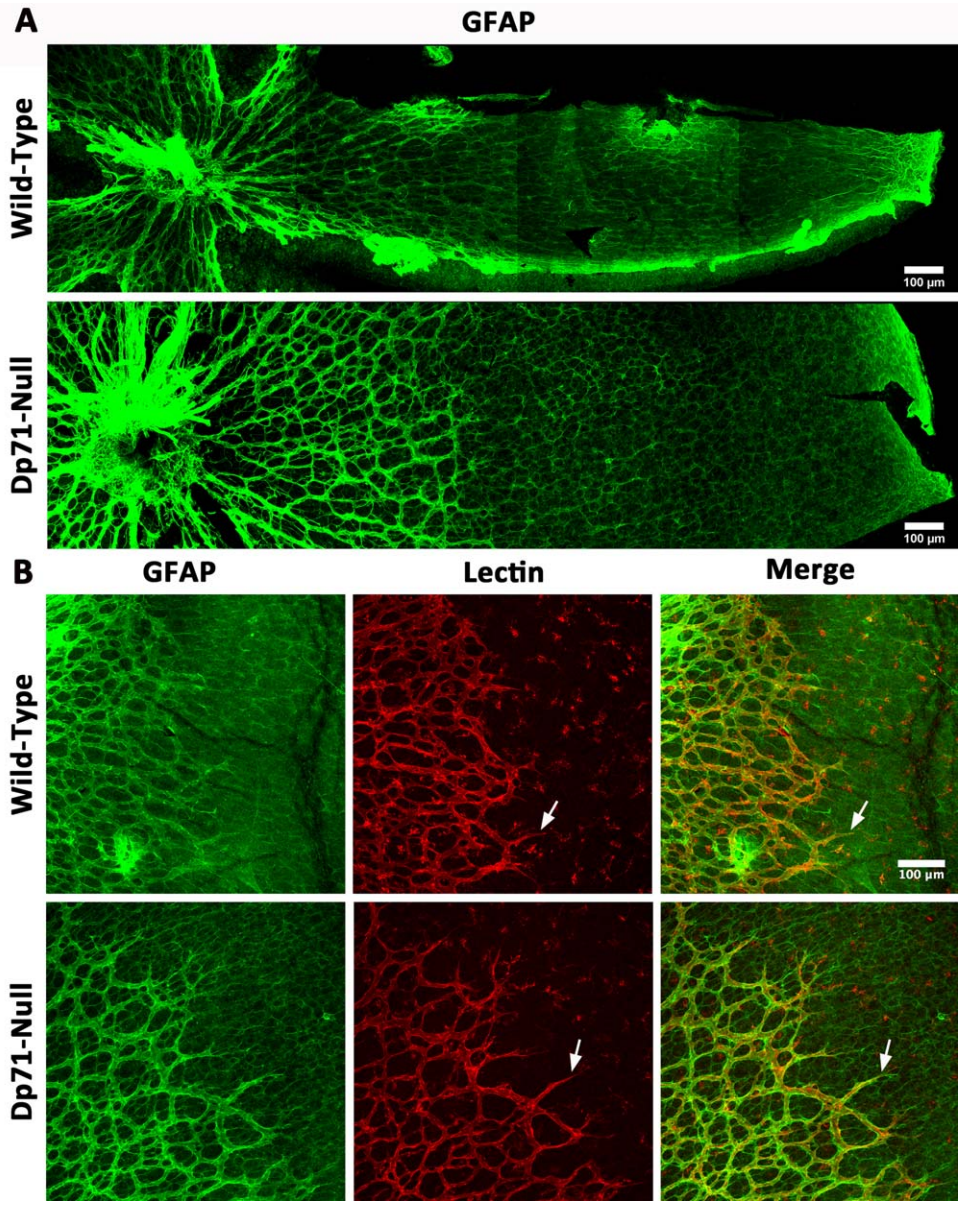

FIGURE 5: Endothelial cells development onto a preexisting astrocyte template (A) Visualization of the astrocyte network labeled with GFAP antibody (*green*) on flat-mount retinas showing that in WT and Dp71-null mice, astrocytes form a complete astrocytic network and are present at the peripheral retina edges from day 3 after birth. (B) Visualization of the astrocyte network labeled with GFAP antibody (*green*) and vascular network labeled with lectin GS (*red*) at postnatal day 3. Merge pictures show that vessels are growing onto a pre-existing astrocyte template. (scale bars = 100 μm).

period. The authors have suggested a potentially direct role of astrocytes in promoting brain angiogenesis through interaction with blood vessels and in particular through their processes due to a close interaction with endothelial cells (Ma et al., 2012). Similarly, in the retina, several studies have shown that the formation of the primary vascular layer is closely associated with the underlying astrocytes that emerge from the optic nerve (Huxlin et al., 1992; Ling et al., 1989; Ling and Stone, 1988; Watanabe and Raff, 1988). Recently, in line with this hypothesis, a study conducted by Fruttiger et al. (1996) has shown that the extent of the astrocyte network assessed by overexpressing PDGF, a mitogen factor for retinal astrocytes (Fruttiger et al., 2000), led to an increase in angiogenesis. Conversely, the loss of astrocyte migration in Tlx knock-out mice was accompanied by the loss of retinal vasculature (Miyawaki et al., 2004).

Here, we analyzed the astrocyte density in Dp71-null mouse retinas from early postnatal stages to adult stage and showed a marked decrease in density compared with WT mice. One day after birth, perinatal mature astrocytes

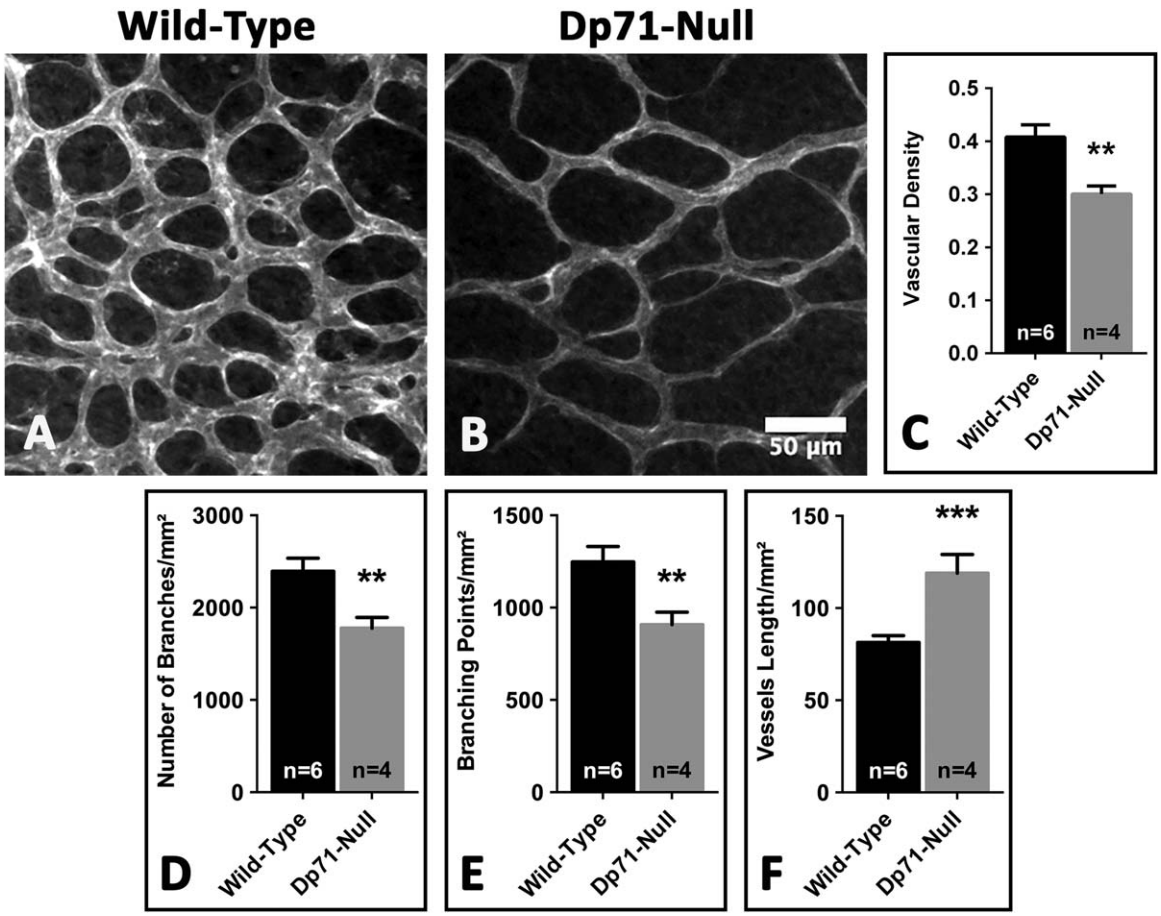

FIGURE 6: Retinal vessel morphology in WT and Dp71-null mouse retinas. (A,B) Visualization of the retinal vascular network labeled with lectin GS at postnatal day 6 in WT (A) and Dp71-null mice (B) (scale bars = 50 μm). (C) Quantification of retinal vessel density using Fiji software. (D) Quantification of the number of retinal vessel branches (D), branching points (E) and total vessel length (F) at P6 ($n = 4$ or 6) using the Analyze Skeleton plugin from Fiji software (see Fig. S1, Supp. Info., same method as for astrocyte quantification).

maintained their proliferative and migratory capacity, but this capacity could be lost thereafter. It has been reported in mouse retina that the termination of developmental apoptosis at approximately P10, seemed to initiate the down-regulation of Bcl-2 family members (Donovan et al., 2006). In Dp71-null mice, the decreased density of astrocytes compared with WT mice could be due to a high rate of astrocyte apoptosis (Chan-Ling et al., 2009). To date, evidence supports a role of Bcl-2 family members and the "classical" mitochondrial caspase-dependent pathway in retinal apoptosis during development (Donovan et al., 2006). We have recently reported that the Bcl-2 mRNA level was increased in Dp71-null mice compared with WT mice (El Mathari et al., 2015). In contrast, the caspase-3 mRNA level did not differ between Dp71-null and WT mice (El Mathari et al., 2015). Based on these findings, we could assume that the *Dp71* gene deletion could lead to retinal compensatory adaptation mechanisms against the greater loss of astrocytes in Dp71-null mice compared with WT mice. It would be interesting to further investigate the upstream signaling events that induce the decrease in astrocyte density in Dp71-null mice.

To the best of our knowledge, this is the first study to show the density of retinal astrocytes and their morphological features in a retina lacking a *DMD* gene product. Indeed, here we also showed that the Dp71 deletion affected not only the density but also strongly the morphology of astrocytes. In the brain of *mdx* mice, Nico et al. (2004) have reported that the Dystrophin Dp71 deficiency altered tight junction biogenesis which is due to the swollen and/or degeneration of perivascular astrocyte end feet in prenatal and postnatal life.

In the retina, we have previously reported that the Müller cell end feet are looser in the absence of Dp71 (Fort et al., 2008). Furthermore as reported (Chase, 1982; Fruttiger, 2007), the deeper retinal plexus is related to Müller glial cells rather than to astrocytes. The morphological change observed in Müller glial cells is probably related to the delayed development of the deeper vascular plexus.

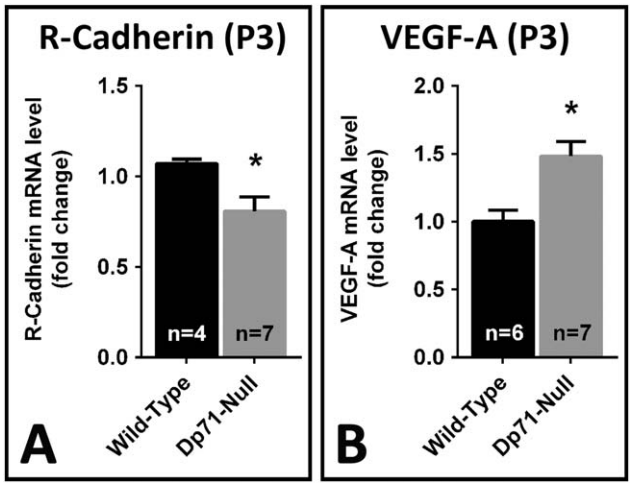

FIGURE 7: R-cadherin and VEGF-A mRNA level in WT and Dp71-null mouse retinas during superficial vasculature plexus formation. R-cadherin (A) and VEGF-A (B) mRNA expression level relative to *β*-actin at P3 in WT and Dp71-null mice. Dp71-null mice express a significantly lower R-cadherin mRNA level at P3 (Mann–Whitney test ± SEM; *$P < 0.05$; $n = 4$ or 7), but also a significantly higher VEGF-A mRNA level at P3 (Mann–Whitney test ± SEM; *$P < 0.05$; $n = 6$ or 7).

Astrocytes show a dynamic plasticity in their distal processes in response to changes in their extracellular environment (Lee et al., 2013, 2014; Renner et al., 2013; Snook et al., 2014; Theodosis et al., 2008). Our *in situ* analysis showed that Dp71-null astrocytes had fewer processes and intersections. These structural changes could decrease the number of astrocyte processes establishing contacts with endothelial cells and neurons. The loss of astrocyte processes is directly linked to leakage of endothelial cell through the down-regulation of tight junctions (Willis et al., 2004a,b). We also quantified the number of times a process segment crossed over a concentric ring (intersections) and we observed that the number of bifurcations decreased significantly in Dp71-null astrocytes compared with WT astrocytes, suggesting a decrease in arbor complexity in these cells. As previously mentioned, the development of the retinal vasculature is preceded by the presence of astrocytes in the retina. They emerge from the optic nerve as a proliferating cell population forming a cellular network that provides a template for blood vessels. As reported by Fruttiger (2007), there is a strict correlation between the presence of astrocytes and blood vessels in the retina. As a consequence, the changes in the fine neuroanatomy of astrocytes observed in Dp71-null mice could be one of the causes of the altered vascular development in these mice associated with a significant decrease in vessel density, number of their branches and branching points compared with WT mice.

All these data are consistent with the observation reported by Acosta et al. (2004) showing that a Dp71 protein deficiency in PC12 cells resulted in an impaired ability of PC12 cells to extend neuritis when incubated with nerve growth factor (NGF) to induce their differentiation (Acosta et al., 2004; Enríquez-Aragón et al., 2005). This deficiency was responsible for a decreased adhesion activity of PC12 cells on different extracellular matrix components such as laminin, collagen, and fibronectin (Enríquez-Aragón et al., 2005).

Laminin is a key component of the ILM throughout development, which could play key roles in its organization. Mice with compound deletion of both the *β2* and *γ3 laminin* genes show ILM disruption (Pinzón-Duarte et al., 2010). In accordance with this finding, we have shown that the absence of Dp71 affects laminins and significantly alters ILM organization (Vacca et al., 2014). Laminins bind to numerous cell-surface receptors, including integrins, dystroglycans, syndecans, and Lutheran blood group glycoproteins (Durbeej, 2010). As dystroglycans are down-regulated in Dp71-null Müller glial cells (Dalloz et al., 2003), it is not surprising that in the absence of Dp71, laminins become disorganized both at the ILM and within the extracellular matrix (Vacca et al., 2014). Anchoring laminins are also essential for the development of a normal retinal vascular network. Indeed, in laminin mutant models (Edwards and Lefebvre, 2013), a highly reduced number of astrocytes, with vessels only present in the peripapillary region has been reported (Gnanaguru et al., 2013). Thus based on this observation, it could be assumed that the visible disorganization of the ILM substantiated by laminin may contribute to the mechanism leading to the delayed development of the primary and deeper vascular plexus as well as the impaired astrocyte network and morphology in Dp71-null retina.

The notion that the primary plexus formation is due to sprouting angiogenesis (Fruttiger, 2002) is supported by the identification of specialized endothelial tip cells at the leading edge of the growing vascular network. They extend long filopodia, suggesting that they could trigger the growth of vascular sprouts as a response to attractant and repellent guidance signals. In our work, we noticed that the deletion of Dp71 did not affect filopodia-like process extension during the development of endothelial cells onto a preexisting astrocyte template (see arrows, Fig. 5B).

VEGF mediates angiogenesis by promoting endothelial cell migration, proliferation, and survival (Ferrara, 2002). But it is also well known as a vascular permeability enhancing factor (Feng et al., 1999). Here, we showed that the deletion of Dp71 was associated with a significantly higher VEGF-A mRNA level at P3 in Dp71-null mouse retinas compared with WT retinas, suggesting that VEGF produced by astrocytes was not directly involved in the angiogenesis delay observed in Dp71-null mice. In the brain, it has been shown

(Nico et al., 2007) that in absence of Dp71, VEGF, and VEGFR-2 were up regulated at both transcriptional and translational levels, in parallel with enhanced HIF-1 mRNA activation in astrocytes and neurons, suggesting the existence of a paracrine loop activated by hypoxia and involving HIF-1, which stimulates VEGF/VEGFR-2 expression leading to compensatory cerebral angiogenesis. Also, in the retina of Dp71-null mice, it has been clearly shown that the absence of Dp71 leads to increased retinal VEGF expression (El Mathari et al., 2015) suggesting that the absence of Dp71 protein leads to increased Müller cell-derived VEGF expression as a compensatory mechanism of the decrease of astrocytes-derived VEGF.

Furthermore, the study of an adhesion molecule known to be involved in neuronal cell guidance, R-cadherin, during the early stages of retinal vascular development has shown that when this specific protein was blocked by a monoclonal anti R-cadherin antibody, the astrocytic template was not affected, unlike the retinal vascularization, suggesting that R-cadherin antibodies could prevent the guidance signals required by endothelial cells to follow the pattern preformed by astrocytes (Dorrell et al., 2002). In accordance with this observation, we showed that R-cadherin was down regulated in absence of Dp71. This could be due to a lower density of retinal astrocytes and vessels given that R-cadherin is known to be responsible for vessel branching in the primary vascular plexus as well as for the proper localization of the deep vascular network.

We have shown previously that the absence of Dp71 decreased the expression of AQP4 protein and induced the redistribution of Kir4.1, initially restricted to the end feet of Müller glial cells along the cell membrane (Dalloz et al., 2003; Fort et al., 2008). Moreover, the absence of Dp71 also leads to a decrease in β-dystroglycan expression around retinal vessels (Dalloz et al., 2003). It has also been demonstrated that the deletion of the *Dp71* gene resulted in a highly permeable inner BRB which is formed by endothelial cells linked together by tight junctions, which separate the neural compartment from the blood (Sagaties et al., 1987), but also by the surrounding pericytes, Müller glial cells and astrocytes (Choi and Kim, 2008; Lee et al., 2011; Toda et al., 2011). Taken together, our data suggest that Dp71 could mediate Müller glial cell, astrocyte and endothelial cell interactions, thus preserving the integrity of the inner BRB (Shen et al., 2010). To date, we have not yet analyzed the impact of Dp71 deletion on the role of pericytes in maintaining the retinal vascular stability. Preliminary data suggest that Dp71 is expressed in mural cells but further investigations are needed to explore the impact of Dp71 deletion on their structure and function.

In this study, we provide evidence that the Dystrophin Dp71, a membrane-associated cytoskeletal protein and the main *DMD* gene product in the retina, regulates astrocyte morphology and density and is associated with subsequent normal blood vessel development. Understanding retinal vascular development is crucial because many retinal vascular diseases such as diabetic retinopathy, retinopathy of prematurity, or BRB disorders that are among the leading causes of blindness are related to the quality of this retinal vascular network. Changes in the fine neuroanatomy of astrocytes observed in Dp71-null mice could be an important upstream factor at the origin of the altered vascular development associated with a significant decrease in vessel density compared with WT mice. Knowing the key role of Dp71 in these mechanisms opens the way for further investigations aiming at identifying intermediate steps involved in angiogenesis in order to identify new therapeutic targets for the treatment of retinal vascular diseases.

Acknowledgment

The authors are grateful to AFM, CONACyT, ECOS Nord, Allergan, Labex, AVOPH, ANR DysTher.

References

Acosta R, Montañez C, Fuentes-Mera L, Gonzalez E, Gómez P, Quintero-Mora L, Mornet D, Alvarez-Salas LM, Cisneros B. 2004. Dystrophin Dp71 is required for neurite outgrowth in PC12 cells. Exp Cell Res 296:265–275.

Aleman V, Osorio B, Chavez O, Rendon A, Mornet D, Martinez D. 2001. Subcellular localization of Dp71 dystrophin isoforms in cultured hippocampal neurons and forebrain astrocytes. Histochem Cell Biol 115:243–254.

Arganda-Carreras I, Fernández-González R, Muñoz-Barrutia A, Ortiz-De-Solorzano C. 2010. 3D reconstruction of histological sections: Application to mammary gland tissue. Microsc Res Tech 73:1019–1029.

Benabdesselam R, Sene A, Raison D, Benmessaoud-Mesbah O, Ayad G, Mornet D, Yaffe D, Rendon A, Hardin-Pouzet H, Dorbani-Mamine L. 2010. A deficit of brain dystrophin 71 impairs hypothalamic osmostat. J Neurosci Res 88:324–334.

Chan-Ling T, Stone J. 1991. Factors determining the migration of astrocytes into the developing retina: Migration does not depend on intact axons or patent vessels. J Comp Neurol 303:375–386.

Chan-Ling T, Chu Y, Baxter L, Weible LM, Hughes S. 2009. In vivo characterization of astrocyte precursor cells (APCs) and astrocytes in developing rat retinae: Differentiation, proliferation, and apoptosis. Glia 57:39–53.

Chase J. 1982. The evolution of retinal vascularization in mammals. A comparison of vascular and avascular retinae. Ophthalmology 89:1518–1525.

Choi YK, Kim KW. 2008. AKAP12 in astrocytes induces barrier functions in human endothelial cells through protein kinase Czeta. Febs J 275:2338–2353.

Claudepierre T, Mornet D, Pannicke T, Forster V, Dalloz C, Bolaños F, Sahel J, Reichenbach A, Rendon A. 2000. Expression of Dp71 in Müller glial cells: A comparison with utrophin- and dystrophin-associated proteins. Invest Ophthalmol Vis Sci 41:294–304.

Dalloz C, Sarig R, Fort P, Yaffe D, Bordais A, Pannicke T, Grosche J, Mornet D, Reichenbach A, Sahel J, Nudel U, Rendon A. 2003. Targeted inactivation of dystrophin gene product Dp71: Phenotypic impact in mouse retina. Hum Mol Genet 12:1543–1554.

Daoud F, Candelario-Martínez A, Billard JM, Avital A, Khelfaoui M, Rozenvald Y, Guegan M, Mornet D, Jaillard D, Nudel U, Chelly J, Martínez-Rojas D, Laroche S, Yaffe D, Vaillend C. 2009. Role of mental retardation-associated dystrophin-gene product Dp71 in excitatory synapse organization, synaptic plasticity and behavioral functions. PLoS One 4:e6574.

Donovan M, Doonan F, Cotter TG. 2006. Decreased expression of pro-apoptotic Bcl-2 family members during retinal development and differential sensitivity to cell death. Dev Biol 291:154–169.

Dorrell MI, Aguilar E, Friedlander M. 2002. Retinal vascular development is mediated by endothelial filopodia, a preexisting astrocytic template and specific R-cadherin adhesion. Invest Ophthalmol Vis Sci 43:3500–3510.

Durbeej M. 2010. Laminins. Cell Tissue Res 339:259–268.

Edwards MM, Lefebvre O. 2013. Laminins and retinal vascular development. Cell Adhes Migr 7:82–89.

El Mathari B, Sene A, Charles-Messance H, Vacca O, Guillonneau X, Grepin C, Sennlaub F, Sahel JA, Rendon A, Tadayoni R. 2015. Dystrophin Dp71 gene deletion induces retinal vascular inflammation and capillary degeneration. Hum Mol Genet 24:3939–3947.

Enríquez-Aragón JA, Cerna-Cortés J, Bermúdez de León M, García-Sierra F, González E, Mornet D, Cisneros B. 2005. Dystrophin Dp71 in PC12 cell adhesion. Neuroreport 16:235–238.

Fabbrizio E, Nudel U, Hugon G, Robert A, Pons F, Mornet D. 1994. Characterization and localization of a 77 kDa protein related to the dystrophin gene family. Biochem J 299:359–365.

Feng Y, Venema VJ, Venema RC, Tsai N, Behzadian MA, Caldwell RB. 1999. VEGF-induced permeability increase is mediated by caveolae. Invest Ophthalmol Vis Sci 40:157–167.

Ferrara N. 2002. Role of vascular endothelial growth factor in physiologic and pathologic angiogenesis: Therapeutic implications. Semin Oncol 29:10–14.

Fort PE, Sene A, Pannicke T, Roux MJ, Forster V, Mornet D, Nudel U, Yaffe D, Reichenbach A, Sahel JA, Rendon A. 2008. Kir4.1 and AQP4 associate with Dp71- and utrophin-DAPs complexes in specific and defined microdomains of Müller retinal glial cell membrane. Glia 56:597–610.

Fruttiger M. 2002. Development of the mouse retinal vasculature: Angiogenesis versus vasculogenesis. Invest Ophthalmol Vis Sci 43:522–527.

Fruttiger M. 2007. Development of the retinal vasculature. Angiogenesis 10: 77–88.

Fruttiger M, Calver AR, Krüger WH, Mudhar HS, Michalovich D, Takakura N, Nishikawa S, Richardson WD. 1996. PDGF mediates a neuron-astrocyte interaction in the developing retina. Neuron 17:1117–1131.

Fruttiger M, Calver AR, Richardson WD. 2000. Platelet-derived growth factor is constitutively secreted from neuronal cell bodies but not from axons. Curr Biol CB 10:1283–1286.

Gariano RF, Gardner TW. 2005. Retinal angiogenesis in development and disease. Nature 438:960–966.

Gnanaguru G, Bachay G, Biswas S, Pinzón-Duarte G, Hunter DD, Brunken WJ. 2013. Laminins containing the $\beta 2$ and $\gamma 3$ chains regulate astrocyte migration and angiogenesis in the retina. Dev Camb Engl 140:2050–2060.

Hirota S, Liu Q, Lee HS, Hossain MG, Lacy-Hulbert A, McCarty JH. 2011. The astrocyte-expressed integrin $\alpha v \beta 8$ governs blood vessel sprouting in the developing retina. Dev Camb Engl 138:5157–5166.

Hirrlinger PG, Pannicke T, Winkler U, Claudepierre T, Varshney S, Schulze C, Reichenbach A, Brunken WJ, Hirrlinger J. 2011. Genetic deletion of laminin isoforms $\beta 2$ and $\gamma 3$ induces a reduction in Kir4.1 and aquaporin-4 expression and function in the retina. PloS One 6:e16106.

Howard PL, Dally GY, Wong MH, Ho A, Weleber RG, Pillers DA, Ray PN. 1998. Localization of dystrophin isoform Dp71 to the inner limiting membrane of the retina suggests a unique functional contribution of Dp71 in the retina. Hum Mol Genet 7:1385–1391.

Huxlin KR, Sefton AJ, Furby JH. 1992. The origin and development of retinal astrocytes in the mouse. J Neurocytol 21:530–544.

Kubota Y, Suda T. 2009. Feedback mechanism between blood vessels and astrocytes in retinal vascular development. Trends Cardiovasc Med 19:38–43.

Lee IS, Lee JE, Kim HJ, Song JW, Choi SH. 2011. Immediate break-down of blood retinal barrier by infusion of triolein emulsion observed by fluorescein angiography. Curr Eye Res 36:358–363.

Lee JC, Ahn JH, Lee DH, Yan BC, Park JH, Kim IH, Cho GS, Kim YM, Lee B, Park CW, Cho JH, Lee HY, Won MH. 2013. Neuronal damage and gliosis in the somatosensory cortex induced by various durations of transient cerebral ischemia in gerbils. Brain Res 1510:78–88.

Lee JC, Ahn JH, Kim IH, Park JH, Yan BC, Cho GS, Ohk TG, Park CW, Cho JH, Kim YM, Lee HY, Won MH. 2014. Transient ischemia-induced change of CCR7 immunoreactivity in neurons and its new expression in astrocytes in the gerbil hippocampus. J Neurol Sci 336:203–210.

Ling TL, Stone J. 1988. The development of astrocytes in the cat retina: Evidence of migration from the optic nerve. Brain Res Dev Brain Res 44:73–85.

Ling TL, Mitrofanis J, Stone J. 1989. Origin of retinal astrocytes in the rat: Evidence of migration from the optic nerve. J Comp Neurol 286: 345–352.

Ma S, Kwon HJ, Huang Z. 2012. A functional requirement for astroglia in promoting blood vessel development in the early postnatal brain. PloS One 7: e48001.

Miyawaki T, Uemura A, Dezawa M, Yu RT, Ide C, Nishikawa S, Honda Y, Tanabe Y, Tanabe T. 2004. Tlx, an orphan nuclear receptor, regulates cell numbers and astrocyte development in the developing retina. J Neurosci Off J Soc Neurosci 24:8124–8134.

Nicchia GP, Nico B, Camassa LM, Mola MG, Loh N, Dermietzel R, Spray DC, Svelto M, Frigeri A. 2004. The role of aquaporin-4 in the blood-brain barrier development and integrity: Studies in animal and cell culture models. Neuroscience 129:935–945.

Nico B, Frigeri A, Nicchia GP, Corsi P, Ribatti D, Quondamatteo F, Herken R, Girolamo F, Marzullo A, Svelto M, Roncali L. 2003. Severe alterations of endothelial and glial cells in the blood-brain barrier of dystrophic mdx mice. Glia 42:235–251.

Nico B, Paola Nicchia G, Frigeri A, Corsi P, Mangieri D, Ribatti D, Svelto M, Roncali L. 2004. Altered blood-brain barrier development in dystrophic MDX mice. Neuroscience 125:921–935.

Nico B, Mangieri D, Crivellato E, Longo V, De Giorgis M, Capobianco C, Corsi P, Benagioano V, Roncali L, Ribatti D. 2007. HIF Activation and VEGF Overexpression are coupled with ZO-1 Up-phosphorylation in the brain of Dystrophic MDX mouse. Brain Pathol 17:399–406.

Pannicke T, Bringmann A, Reichenbach A. 2002. Electrophysiological characterization of retinal Müller glial cells from mouse during postnatal development: Comparison with rabbit cells. Glia 38:268–272.

Pinzón-Duarte G, Daly G, Li YN, Koch M, Brunken WJ. 2010. Defective formation of the inner limiting membrane in laminin beta2- and gamma3-null mice produces retinal dysplasia. Invest Ophthalmol Vis Sci 51:1773–1782.

Provis JM, Sandercoe T, Hendrickson AE. 2000. Astrocytes and blood vessels define the foveal rim during primate retinal development. Invest Ophthalmol Vis Sci 41:2827–2836.

Renner NA, Sansing HA, Inglis FM, Mehra S, Kaushal D, Lackner AA, Maclean AG. 2013. Transient acidification and subsequent proinflammatory cytokine stimulation of astrocytes induce distinct activation phenotypes. J Cell Physiol 228:1284–1294.

Sagaties MJ, Raviola G, Schaeffer S, Miller C. 1987. The structural basis of the inner blood-retina barrier in the eye of Macaca mulatta. Invest Ophthalmol Vis Sci 28:2000–2014.

Sarig R, Mezger-Lallemand V, Gitelman I, Davis C, Fuchs O, Yaffe D, Nudel U. 1999. Targeted inactivation of Dp71, the major non-muscle product of the DMD gene: Differential activity of the Dp71 promoter during development. Hum Mol Genet 8:1–10.

Schnitzer J. 1988. Immunocytochemical studies on the development of astrocytes, Müller (glial) cells, and oligodendrocytes in the rabbit retina. Brain Res Dev Brain Res 44:59–72.

Scott A, Powner MB, Gandhi P, Clarkin C, Gutmann DH, Johnson RS, Ferrara N, Fruttiger M. 2010. Astrocyte-derived vascular endothelial growth factor stabilizes vessels in the developing retinal vasculature. PloS One 5:e11863.

Sene A, Tadayoni R, Pannicke T, Wurm A, El Mathari B, Benard R, Roux MJ, Yaffe D, Mornet D, Reichenbach A, Sahel JA, Rendon A. 2009. Functional implication of Dp71 in osmoregulation and vascular permeability of the retina. PloS One 4:e7329.

Shen W, Li S, Chung SH, Gillies MC. 2010. Retinal vascular changes after glial disruption in rats. J Neurosci Res 88:1485–1499.

Snook ER, Fisher-Perkins JM, Sansing HA, Lee KM, Alvarez X, MacLean AG, Peterson KE, Lackner AA, Bunnell BA. 2014. Innate immune activation in the pathogenesis of a murine model of globoid cell leukodystrophy. Am J Pathol 184:382–396.

Stone J, Itin A, Alon T, Pe'er J, Gnessin H, Chan-Ling T, Keshet E. 1995. Development of retinal vasculature is mediated by hypoxia-induced vascular endothelial growth factor (VEGF) expression by neuroglia. J Neurosci 15:4738–4747.

Stenzel D, Lundkvist A, Sauvaget D, Busse M, Graupera M, van der Flier A, Wijelath ES, Murray J, Sobel M, Costell M, Takahashi S, Fässler R, Yamaguchi Y, Gutmann DH, Hynes RO, Gerhardt H. 2011. Integrin-dependent and -independent functions of astrocytic fibronectin in retinal angiogenesis. Dev Camb Engl 138:4451–4463.

Szabó A, Jancsik V, Mornet D, Kálmán M. 2004. Immunofluorescence mapping of dystrophin in the rat brain: Astrocytes contain the splice variant Dp71f, but this is confined to subpopulations. Anat Embryol (Berl) 208:463–477.

Theodosis DT, Poulain DA, Oliet SHR. 2008. Activity-dependent structural and functional plasticity of astrocyte-neuron interactions. Physiol Rev 88:983–1008.

Toda R, Kawazu K, Oyabu M, Miyazaki T, Kiuchi Y. 2011. Comparison of drug permeabilities across the blood-retinal barrier, blood-aqueous humor barrier, and blood-brain barrier. J Pharm Sci 100:3904–3911.

Vacca O, Darche M, Schaffer DV, Flannery JG, Sahel JA, Rendon A, Dalkara D. 2014. AAV-mediated gene delivery in Dp71-null mouse model with compromised barriers. Glia 62:468–476.

Watanabe T, Raff MC. 1988. Retinal astrocytes are immigrants from the optic nerve. Nature 332:834–837.

Wersinger E, Bordais A, Schwab Y, Sene A, Bénard R, Alunni V, Sahel JA, Rendon A, Roux MJ. 2011. Reevaluation of dystrophin localization in the mouse retina. Invest Ophthalmol Vis Sci 52:7901–7908.

West H, Richardson WD, Fruttiger M. 2005. Stabilization of the retinal vascular network by reciprocal feedback between blood vessels and astrocytes. Dev Camb Engl 132:1855–1862.

Willis CL, Leach L, Clarke GJ, Nolan CC, Ray DE. 2004a. Reversible disruption of tight junction complexes in the rat blood-brain barrier, following transitory focal astrocyte loss. Glia 48:1–13.

Willis CL, Nolan CC, Reith SN, Lister T, Prior MJW, Guerin CJ, Mavroudis G, Ray DE. 2004b. Focal astrocyte loss is followed by microvascular damage, with subsequent repair of the blood-brain barrier in the apparent absence of direct astrocytic contact. Glia 45:325–337.